Electronic Supplementary Material (ESI) for Reaction Chemistry & Engineering.

SUPPLEMENTARY MATERIAL:
Energetics of Cellulose and Cyclodextrin Glycosidic Bond Cleavage

Cheng Zhu[1], Christoph Krumm[1], Gregory Facas[1], Matthew Neurock[1], Paul J. Dauenhauer[1,*]

[1]Department of Chemical Engineering and Materials Science, University of Minnesota, 421 Washington Ave. SE, 484 Amundson Hall, Minneapolis, MN, 55455

Table of Contents

S1. Design and Validation of PHASR Reactor

The PHASR (Pulse Heated Analysis of Solid Reactions) reactor is an analytical tool designed to probe high-temperature millisecond-scale reactions on laboratory-scale. We present the detailed design of the PHASR reactor. PHASR design includes microreactor assembly, 1.0 kHz control system integration, cooling system design, and analytical instrument integration.

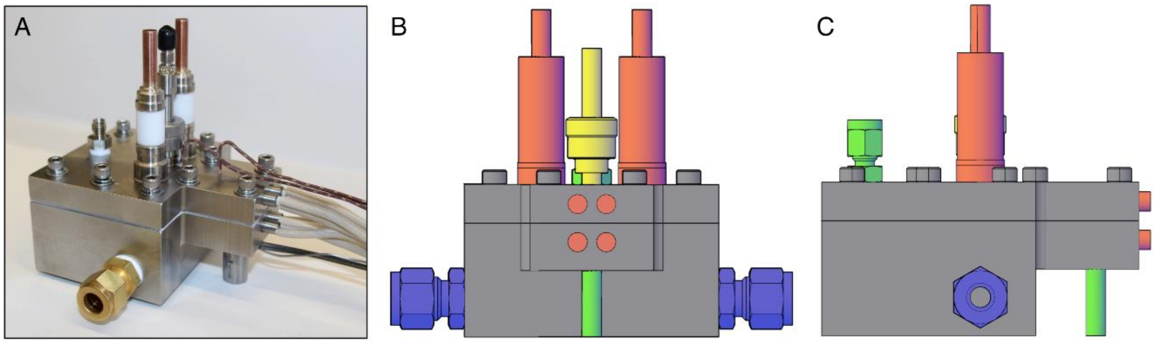

Figure S1. PHASR Reactor. The PHASR reactor is a laboratory-scale analytical device designed to rapidly heat and cool samples on a millisecond timescale via resistive heating and high-power cooling, thereby allowing for measurement of high temperature, sub-second reaction kinetics.

S1.1. PHASR Reactor Design

The PHASR reactor assembly consists of two stainless steel custom machined blocks – the upper heating block and a lower cooling block – which close together to form the reaction chamber. The heating contains two copper electrical feedthroughs that transfer uniform electrical current to heat the steel heating element, which holds the cellulose sample. The cooling block consists of a micro-machined heat exchanger through which a high velocity coolant is pumped to achieve sample cooling. The two reactor halves are sealed together with a custom-cut Teflon gasket, thereby forming a channel through which helium carrier gas flows (200 sccm) to rapidly inject products into the GC inlet. In order to prevent condensation of semi-volatile products, the entire reactor block is heated via five cartridge heaters.

S1.2. PHASR System Design

The PHASR reactor is controlled via three sub-systems working in unison: (1) power loop with millisecond PID feedback control, (2) cooling loop with high-flow booster pump, and (3) fully-integrated GC-MS analysis. After a sample is loaded, a PHASR reaction is initiated by the power supply system, which resistively heats the sample for the desired temperature and duration. The cooling loop flows high velocity coolant through the heat exchanger such that sample is rapidly cooled when the power supply shuts off. Finally, continuously flowing helium carrier gas sends gas and volatile products from the reactor directly into the GC inlet.

The power loop consists of a power supply with integrated 2000 Hz controller and a transformer which converts 480 volt inlet power to 13 volt direct current up to 2000 amps. Feedback temperature control is achieved with an optical pyrometer with optical light pipe probe, which measures the sample temperature at 1000 Hz, and outputs a 0-20 milliamp signal, which is converted to 0-10 volt for feedback to the power supply controller.

The cooling loop consists of a circulating chiller bath and a high-flow gear pump, which acts as a booster to achieve high flow during a PHASR reaction. Due to the high temperatures present during a reaction, a high temperature silicon-based heat transfer fluid (DOW, Syltherm-800) is used to prevent film boiling, which would reduce heat transfer from the heating element. The closed-loop system is connected with 3/8-inch copper tubing and stainless steel fittings.

The PHASR system is integrated with an Agilent 7890A gas chromatograph with TCD, FID, and a switching valve similar to previous work as well as an Agilent 220 ion trap mass spectrometer. The PHASR reactor is spliced directly into the stainless steel lines between the helium inlet EPC and the inlet, such that the helium carrier gas flows directly through the reactor channel and into the GC inlet.

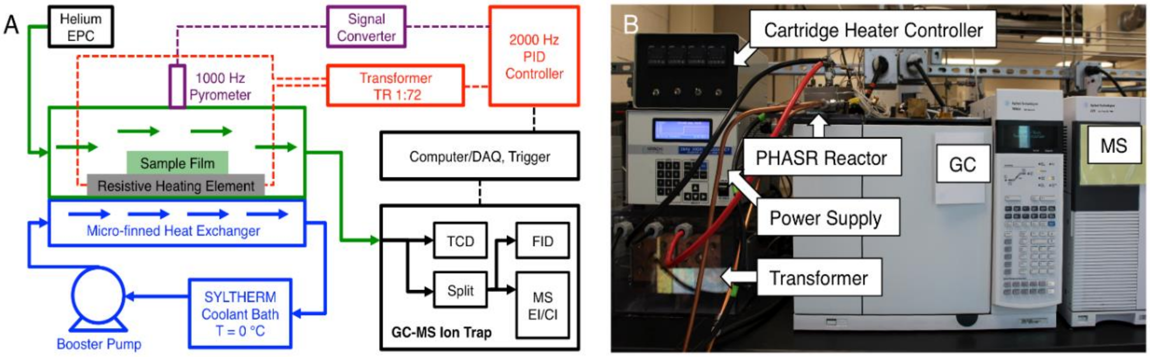

Figure S2. PHASR Systems Integration. A. A schematic of the overall system shows the layout of the 1000 Hz PID heating controller, high velocity coolant loop, and direct integration with analytical equipment. **B.** A photo of the PHASR systems assembly, with the reactor directly integrated with the gas chromatograph inlet.

S1.3. Validation of PHASR

The PHASR reactor system was designed to probe the kinetics of high temperature reactions on a millisecond scale. By employing resistive heating with 1000 Hz feedback control in tandem with a high velocity heat transfer fluid, the PHASR microreactor heats and cools feedstocks in pulses on a millisecond timescale, thereby portioning the formation of products into segments for subsequent analysis via integrated GC-MS. Reactor geometry was optimized via three-dimensional fluid dynamics simulation to ensure rapid injection of gas and volatile products to the GC. When used to study cellulose pyrolysis, the PHASR system can effectively measure rates of formation of individual pyrolysis products in a reaction-dominant, isothermal system.

The flow path measured via COMSOL fluid dynamics simulation, shown in Figure S3B, shows highly linear helium streamlines through the PHASR reactor channel. Due to the narrow height of the channel, helium flow remains laminar (low Re), thereby ensuring negligible loss in GC peak resolution. With a gas-phase residence time across the heating element fewer than 10 milliseconds, pyrolysis products were rapidly quenched and injected onto the GC column. Rapid transfer of products from the PHASR to the gas chromatograph ensures negligible reaction of volatile products in the gas phase.

A major design consideration for the PHASR reactor was to ensure collection of isothermal data. As such, heating and cooling of the reactant sample must be sufficiently fast such that minimal reaction of reaction occurs during the heating or cooling phase. Targets for maximum allowable heating and cooling time were developed using a thermally resolved microkinetic model based on the lumped Broido-Shafizadeh kinetic[40] yielded target heating and cooling times of 50 and milliseconds 250 milliseconds respectively. These targeted heating and cooling times yielded minimal formation of volatile products (<5%) during each phase at 500 °C [23]. Primary experimental validation was conducted by measuring heating and cooling rates for comparison with the kinetic model benchmarks determined from the kinetic model. Shown in Figure S4A, the PHASR reactor was capable of heating to 500 °C in fewer than 35 ms and cooling in fewer than 150 ms.

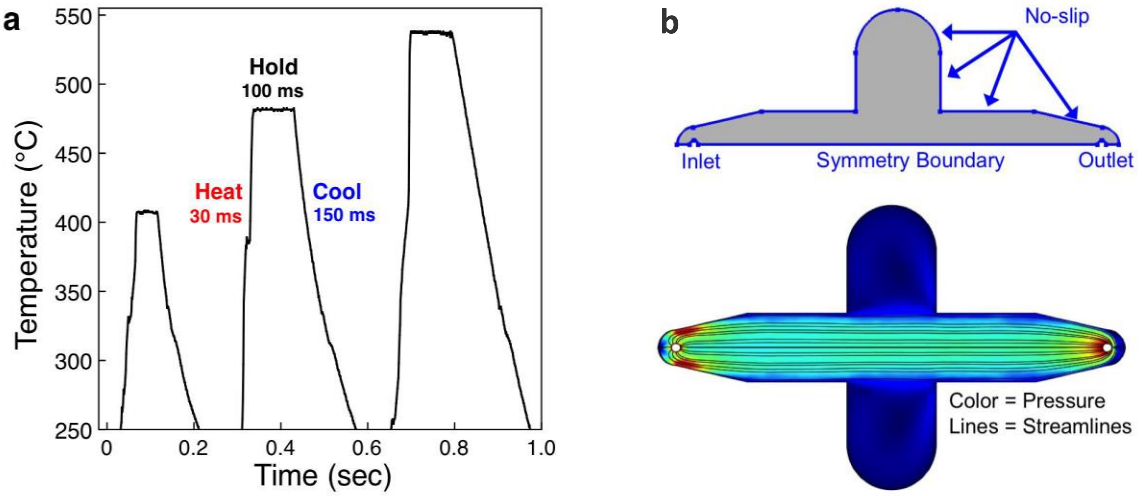

Figure S3. PHASR Results. A. Temperature-time profiles generated using the PHASR reactor show capability to heat in less than 35ms and cool in under 150ms. **B.** A COMSOL flow simulation with prescribed boundary conditions shows a highly linear helium flow path through the reactor, ensuring rapid transfer of gas and volatile products to the gas chromatograph.

For more information regarding detailed assembly of each sub unit, CAD drawings and individual part information for the PHASR system, refer to the supporting information of reference number 23 in the main paper.

S2. α-Cyclodextrin as Surrogate for Cellulose

To identify a low molecular weight surrogate which generates pyrolysis product yields similar to cellulose, the thin-film pyrolysis product distributions of glucose, cellehexaose and α-cyclodextrin were determined. Results yielded large differences between glucose, cellohexaose, and cellulose [22]. The product distribution of α-Cyclodextrin matches the pyrolysis product distribution of cellulose well, at temperatures between 400-600 ^{0}C and in powder pyrolysis with only formic acid differing significantly. Previous work has also shown that no significant differences in pyrolysis product distribution between α linkages seen in α-cyclodextrin and β linkages seen in cellulose. Further confirming the validity for cyclodextrin use as a cellulose surrogate.

S3. Characterization of Gas Phase Products

To analyze product formation rates, gas and volatile products were rapidly transferred from the PHASR reactor to the GC-MS via helium sweep gas, which is also used as a carrier gas for separation. The gas chromatograph method used for separation, quantification, and identification is outlined in Table S1.

Table S1. Agilent GC-MS Method details for separation and identification of gas and volatile products from the PHASR reactor.

Gas Chromatograph Method	
Inlet Temperature	300 °C
Inlet He Pressure	30 psi for 2 min, then 14 psi
Inlet Split Ratio	10:1
Inlet Septum Purge	3 mL/min
Oven Ramp	-30 °C to 260 °C in 70 min, hold 20 min
Valve Switch	All products to FID/MS after 2 min
Mass Spectrometer (EI mode)	Scan range m/Z 44 to 320

All products were identified by matching retention times with purchased calibration standards, as well as identification via EI mass spectrometry. Table S2 lists retention times and primary ion fragments for all eight furan-based compounds. Calibration of compounds was performed by matching FID peak areas with known quantities of calibration standard for every GC analyte.

Table S2. GC retention times and major ions from EI mass spectrometry for all eight furan-based products presented in the main paper.

Compound	**Structure**	**Retention Time**	**Molar Mass**	**Major Ion Fragments**		
				Ion	**Relative Height**	**Fragment Lost**
Furan	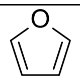	10.73	68	82	999	-
2-methylfuran	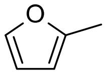	18.3	82	68	999	-
				53	905	-CHO
				81	854	- H
2,5-dimethylfuran	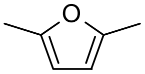	27.53	96	96	999	-
				95	987	-H
				53	863	-C2H3O
furfural	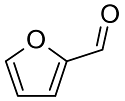	37.51	96	96	693	-
				95	999	-H
2-furanmethanol	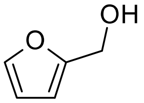	39.68	98	98	999	-
				97	619	-H
				81	53	-OH
				69	614	-CHO
				53	831	-45
2(5H)Furanone	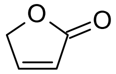	44.75	84	84	286	-
				55	999	-CHO
5-methylfurfural	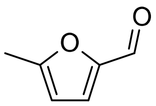	48.7	110	110	739	-
				109	747	-H
				53	999	-57
				51	503	-59
5-hydroxymethyl furfural	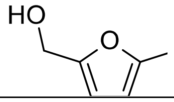	65.43	126	126	279	-
				97	999	-CHO

				69	803	-57

S4. Tabulated Cyclodextrin Conversion Data

The following tables contain raw data presented in the main paper, including time resolved data and Arrhenius plots for α-cyclodextrin conversion. Table S3 shows the evolution of α-cyclodextrin conversion with different pulse length (20 to 2000 ms) for the range of temperatures (385 to 505 °C).

Table S3. Cyclodextrin Conversion at Different Temperatures. Thin-Film samples of α-cyclodextrin were exposed to thermal pulses varying from 20 ms to 2000 ms at temperatures varying from 385 °C to 505 °C.

Temperature [°C]	**385**		**400**		**415**	
Pulse Length [ms]	**Conversion [%]**	**Error [%]**	**Conversion [%]**	**Error [%]**	**Conversion [%]**	**Error [%]**
20	1.38	1.91	1.42	1.85	1.97	3.23
50	4.08	2.19	3.08	4.41	6.23	0.32
75	3.81	3.56	7.72	4.02	9.49	5.16
100	4.22	3.31	7.57	5.76	7.79	7.90
150	6.44	3.56	8.85	4.89	12.49	4.95
200	10.12	2.73	14.75	5.88	18.27	1.98
500	20.23	5.97	21.97	1.95	33.80	7.84
1000	36.35	10.11	39.50	6.17	55.12	4.79
2000	55.41	7.20	61.50	12.03	76.00	2.37
Temperature [°C]	**430**		**445**		**460**	
Pulse Length [ms]	**Conversion [%]**	**Error [%]**	**Conversion [%]**	**Error [%]**	**Conversion [%]**	**Error [%]**
20	2.82	3.22	4.25	2.19	5.70	1.67
50	9.57	4.57	9.11	4.67	12.98	4.19
75	9.61	4.62	12.82	1.78	16.98	3.81
100	13.03	2.12	15.11	6.11	24.36	5.11
150	18.78	3.74	23.66	4.47	28.78	13.43
200	22.36	8.00	29.26	4.78	42.81	2.97
500	52.36	5.21	60.09	3.81	71.68	7.70
1000	75.60	5.53	81.29	7.34	90.56	6.49
2000	94.06	5.28	95.18	5.99	97.14	3.56
Temperature [°C]	**475**		**490**		**505**	
Pulse Length [ms]	**Conversion [%]**	**Error [%]**	**Conversion [%]**	**Error [%]**	**Conversion [%]**	**Error [%]**
20	9.87	5.20	13.68	3.39	28.79	7.98
50	21.49	3.66	33.77	2.65	61.53	3.87
75	43.05	7.60	43.78	1.59	78.20	2.74

100	41.81	5.53	63.64	9.56	87.48	4.33
150	52.64	6.05	74.32	9.45	92.43	2.38
200	60.36	5.75	87.52	9.73	94.23	1.91
500	89.21	8.16	95.67	5.68	99.14	4.80
1000	95.97	3.14	97.23	4.37	99.16	3.23
2000	98.02	1.15	98.91	2.73	99.28	0.73

Table S4 shows the reaction rate constants of α-cyclodextrin conversion fitted from first-order kinetics for temperatures from 385 to 505 °C.

Table S4. Arrhenius Data for Cyclodextrin Conversion. Reaction rate coefficients are reported as s^{-1} at temperatures from 385 °C to 505 °C.

Temperature [°C]	**385**	**400**	**415**	**430**	**445**	**460**	**475**	**490**	**505**
k [1/s]	0.42	0.49	0.74	1.41	1.71	2.41	4.60	9.73	20.33
k, lower [1/s]	0.32	0.36	0.67	1.12	1.40	1.89	3.54	7.37	17.87
k, upper [1/s]	0.53	0.66	0.82	1.72	2.15	2.96	5.68	12.44	23.58

Supplementary Information References

23. C. Krumm, J. Pfaendtner, P.J. Dauenhauer, "Millisecond pulsed films unify the mechanisms of cellulose fragmentation," Chemistry of Materials 2016, DOI: 10.1021/acs.chemmater.6b00580

40. A.G.W. Bradbury, Y. Sakai, F. Shafizadeh, "A kinetic model for pyrolysis of cellulose," J. of Applied Polymer Science 1979, 23, 3271-3280.

22. M.S. Mettler, S.H. Mushrif, A.D. Paulsen, A.D. Javadekar, D.G. Vlachos, P.J. Dauenhauer, "Revealing pyrolysis chemistry for biofuels production: Conversion of cellulose to furans and small oxygenates," *Energy and Environmental Science* 2012, 5, 5414.